


Article

Adsorption of Orange G in Liquid Solution by the Amino Functionalized GO

Zhiquan Yang , Chong He, Wenning Liao, Xinyi Zhang, Wanhui Liu and Baosheng Zou

School of Environment and Energy, South China University of Technology, Guangzhou Higher Education Mega Centre, Guangzhou 510006, China

* Correspondence: zqyang@scut.edu.cn; Tel.: +86-186-2050-7019

Abstract: Dye effluent damaged the water environment and human health with its massive discharge. In order to eliminate dye from the water environment, a variety of adsorbents were used to investigate dye removal. Graphene oxide (GO) attracted extensive attention due to its excellent surface property in the degradation of dye wastewater. Modified GO with multifunctional groups helped to improve adsorption performance. 3-Aminopropyltriethoxysilane modified GO (AS-GO) was fabricated for the removal of Orange G (OG) in this study. The results showed that AS-GO had an excellent adsorption ability of OG. During the reaction process, the maximum adsorptive capacity of OG was up to 576.6 mg/g at $T = 313\text{ K}$ and $\text{pH} = 3$ with the initial OG concentration of 100 mg/L and the initial adsorbent dose of 2.5 g/L. The adsorption kinetic process of AS-GO conformed to the pseudo-second-order and Langmuir models. The spontaneous and endothermic adsorption of OG occurred in the adsorption process. The main adsorption mechanisms were electrostatic, π - π and hydrogen bonding interactions in the reaction process. After four cycles of AS-GO, it maintained high removal efficiency owing to its remarkable stability. The scheme of GO modified with AS could hinder the agglomeration of GO and provide more active sites, which would further enhance the adsorption properties and expand its application in water purification.

Keywords: adsorption; Orange G; graphene oxide; 3-aminopropyltriethoxysilane



Citation: Yang, Z.; He, C.; Liao, W.; Zhang, X.; Liu, W.; Zou, B.

Adsorption of Orange G in Liquid Solution by the Amino Functionalized GO. *Separations* **2022**, *9*, 391. <https://doi.org/10.3390/separations9120391>

Academic Editor: Gavino Sanna

Received: 11 October 2022

Accepted: 21 November 2022

Published: 24 November 2022

Publisher's Note: MDPI stays neutral with regard to jurisdictional claims in published maps and institutional affiliations.



Copyright: © 2022 by the authors. Licensee MDPI, Basel, Switzerland. This article is an open access article distributed under the terms and conditions of the Creative Commons Attribution (CC BY) license (<https://creativecommons.org/licenses/by/4.0/>).

1. Introduction

Due to the wide application in the dyeing and printing of textiles, paper, paint and other fields [1,2], dyes had been counted as one of the dominating contaminants in the hydrographic condition [3]. Dyes can cause some considerable problems, such as the endangerment of human health, staining of water, and destruction of the ecological environment [4]. As one of commonly used dyes in the world, azo dyes had lethality, genotoxicity and oncogenicity on the creatures [5]. People's gastrointestinal and respiratory tract also might be irritated if they are exposed to azo dyes sequentially [6]. Thus, dyeing effluent needed to be decontaminated before it was discharged.

Various technologies, such as advanced oxidation, chemical coagulation, aerobic process, anaerobic process and adsorption [5–9], have been used to remove OG in wastewater. Conventionally, chemical coagulation was used to separate suspended matter and remove dye contaminant in wastewater. However, the production of large amounts of sludge limited its application. Biological treatment was cheaper and more environmentally friendly than physical methods, but high dye concentration inhibited bacterial activity. Although advanced oxidation had high efficiency and short reaction time, the cost of chemicals was high [10]. Adsorption, an effective and economically feasible method, was often selected in practical applications [11]. Many adsorbents, such as alumina nanoparticles [12], activated carbon [13], MOFs [14], layered double hydroxide [15], etc., had been designed to remove dyes. Abdelkader et al. [7] synthesized Mg-Fe bimetallic hydroxide to remove OG in simulated wastewater, and the good adsorption efficiency (approximately 300 mg/g) could be

kept at the pH range of 3–13. Two β -cyclodextrin polymers modified with different amide groups were reported to achieve good adsorption efficiency of Congo Red and OG (813, 442 and 40,446 mg/g, respectively) [16]. However, low adsorption capacity and stability limited the practical applications of these materials. There is an urgent need for adsorbent with high adsorption capacity in the wastewater treatment.

GO has been extensively used in the adsorption of organic contaminants and heavy metals in liquid solution as a result of its big specific surface area and ample oxygen species [17,18]. However, some defects, such as easy reunion and hard recycle, limited its practical application. Various functionalized GO was investigated to improve its property [19]. Ethylenediamine triacetic acid-GO (ETDA-GO) had a better adsorption efficiency of Pb (II) than GO (from 367 to 525 mg/g) [20]. Wang et al. synthesized graphene oxide modified by persimmon tannin to remove methyl blue in aqueous solution, and the maximal adsorption capacity achieved 256.58 mg/g [21]. The amine groups ($-\text{NH}_2$) could enhance the materials' adsorptive property due to the increase in adsorption sites [22]. 3-Aminopropyltriethoxysilane (AS) was an important agent for the introduction of $-\text{NH}_2$. Both AS-functionalized biopolymers chitin (CTN) and chitosan (CTS) had a fast adsorption rate, short equilibrium time, and great recyclability [23]. We selected it as a modified material to hinder the agglomeration of GO. There are no reports about the removal of OG in water by the AS-GO.

The objective was to present a study of the adsorption of OG on AS-GO in water. Influence factors such as initial solution pH, adsorbent dosage, temperature, and coexisting ion were studied in detail. Then, a primary adsorption mechanism was presented in detail. Finally, the regenerability and stability were also discussed. This research aims to leverage the advantages of AS-functionalized GO to overcome the shortcomings and achieve the following innovations: (1) the introduction of AS reduced the reunion of GO; (2) a large number of amino functional groups were introduced through covalent bonding to improve the adsorption performance of functionalized materials; (3) the hydrophilicity of GO was helpful to its dispersibility in water.

2. Experimental

2.1. Reagents

OG and AS ($\text{AS} \geq 98\%$), as well as graphite powder (750–850 mesh), were provided by Aladdin (Shanghai, China). A fixed amount of OG was dissolved in deionized water to form a 1000 mg/L OG stock solution. All reagents are of analytical grade.

2.2. Preparation of AS-GO

GO was prepared according to the modified Hummers method [24,25]. Then, 100 mL GO (3.5 g/L) and 100 mL absolute ethanol were mixed in a flask and sonicated for 1 h. After, 3.5 mL AS was added to the above dispersion, and it was heated up to 70 °C at 1800 rpm/min under the magnetic stirring for 4 h. After the mixture was cooled to indoor temperature, the suspended solids were isolated, washed and dried at 60 °C. Then, AS-GO was obtained.

2.3. Adsorption Experiment

AS-GO adsorption tests were carried out in a batch system under the following conditions [26]. First, 0.02 g AS-GO and 250 mL OG solutions (100 mg/L) at pH 3.0 were added in conical flasks. The conical flask was sealed and placed in a thermostatic shaker at a temperature of 298 K and a rotational speed of 160 rpm for 24 h. After the reaction was finished, the mixture was filtered through a 0.22 μm syringe filter, and then, the concentration of remaining OG was determined at 475 nm by UV-vis spectrophotometry (Model UV-vis 756, Shanghai Jinghua Instruments Co., Ltd., Shanghai, China). The complex with the adsorbed OG (AS-GO-OG) could be obtained by centrifuging and drying directly after reaction. After the adsorption process, adsorbent was centrifuged, rinsed, dried and

recycled in the fresh OG solution under the same condition for another 3 cycles to evaluate the regeneration of AS-GO.

2.4. Data Analysis

The pseudo-first-order kinetics can be expressed by the following formula (Equation (1)):

$$\log (q_e - q_t) = \log q_e - k_1 t / 2.303 \quad (1)$$

The pseudo-second-order kinetics can be expressed by the following formula (Equation (2)):

$$t / q_t = 1 / k_2 q_e^2 + t / q_e \quad (2)$$

where q_e and q_t are the adsorption capacity (mg/g) of AS-GO to OG at equilibrium and t time (min). k_1 and k_2 are the rate constant of the pseudo-first-order and pseudo-second-order kinetic equation ($\text{g} \cdot \text{mg}^{-1} \text{ min}^{-1}$). The experimental data were linearly fitted, and the horizontal and vertical coordinates were t and t/q_t , respectively, and k_1 , k_2 and q_e were calculated based on the intercept and slope.

The equation of the Langmuir adsorption isotherm model can be expressed as follows (Equation (3)):

$$q_e = q_{\max} K_L C_e / (1 + K_L C_e) \quad (3)$$

The equation of the Freundlich adsorption isotherm model can be expressed as follows (Equation (4)):

$$q_e = K_F C_e^{1/n} \quad (4)$$

q_e and C_e are the equilibrium adsorption amount (mg/g) and solution concentration (mg/L) when the reaction reaches equilibrium. K_F and n are Freundlich constants. The former is related to the adsorption capacity, and the unit is L/mg. The latter is related to the adsorption strength. The n value can usually be used to judge the difficulty of the adsorption process: when $0.1 < 1/n < 1$, adsorption is easy; when $1/n > 1$, adsorption is difficult.

The thermodynamic model can be presented via the subsequent formula (Equations (5) and (6)):

$$\Delta G = -RT \ln K_p \quad (5)$$

$$\ln K_p = \Delta H / (RT) + \Delta S / R \quad (6)$$

in which $K_p = q_e / C_e$, where q_e and C_e are the equilibrium adsorption quantity and solution concentration, respectively, when the adsorption reached equilibrium, R is the gas constant ($8.314 \text{ J} \cdot \text{mol}^{-1} \cdot \text{K}^{-1}$), and T is thermodynamic temperature (K).

2.5. Characterization Methods

FTIR (Fourier Transform infrared spectroscopy) was measured in KBr pellet to research the functional groups. X-ray diffraction (XRD) was applied to analyze the structure of AS-GO before and after adsorption. In addition, XRD patterns were recorded with a Bruker D8 advance diffractometer (Karlsruhe, Germany) according to Cu-K α radiation ($\lambda = 1.5418 \text{ \AA}$).

3. Results and Discussion

3.1. Removal Experiments

3.1.1. Effect of Initial pH

The surface charge distribution of AS-GO and the form of pollutants were related to the initial pH, so it was imperative to consider the influence of the initial pH of the solution. The test on the effect of pH (from 1.0 to 8.0) was carried out (Figure 1). The adsorption capacity of OG increased with the promotion of pH (at the range of pH = 1–3) and achieved up to 418.4 mg/g at pH 3.0. Then, the adsorption capacity decreased with the promotion of pH from 3 to 8.

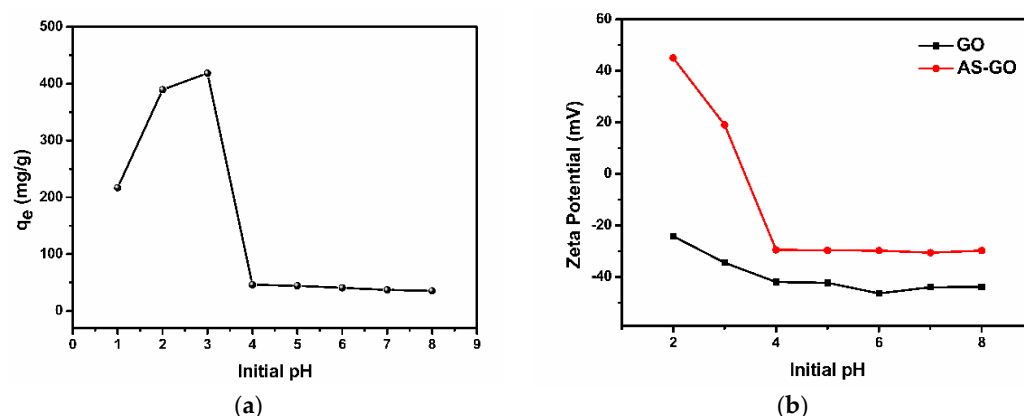


Figure 1. (a) Effect of pH on the removal of OG by AS-GO, (b) Zeta potential of GO and AS-GO.

The pH effect on OG removal could be related to the surface charge of the adsorbent and the species of OG in solution. The zeta potential value (Figure 1b) demonstrated that the surface charge of adsorbent was positive at $\text{pH} < 3.0$ [26]. Anionic OG was the main form in acidic solution [27]. The amino functional group ($-\text{NH}_2$) of AS-GO might transform into a positively charged group ($-\text{NH}_3^+$) by protonation and lead to electrostatic interaction with the negatively charged sulfonic acid group (SO_3^-) in OG. At $\text{pH} > 4.0$, the protonated amino functional groups decreased and the OH^- amount gradually increased. Electrostatic interaction was weakened. When the zeta potential of AS-GO was negative, the adsorption capacity was decreased to 40 mg/g. These indicated that another reaction mechanism existed in the reaction system besides electrostatic interaction. To sum up, the electrostatic interaction between $-\text{NH}_3^+$ and SO_3^- in OG was one of the adsorption mechanisms. The forthcoming experiments took place at $\text{pH} = 3.0$.

3.1.2. Effect of Adsorbent Dose

Adsorbent dose also affected the adsorption process (Figure 2). When the adsorbent dose augmented from 0.1 to 0.35 g/L, the removal rate improved from 49.86% to 94.68%. This could be explained that the higher dose of adsorbent provided the more adsorption sites [28]. Adsorption capacity showed a steady decrease from 498.6 to 270.5 mg/g with the augment of adsorbent dose. The utilization rate of the adsorption site was decreased with the increasing adsorbent dose. In order to achieve the maximum utilization of the adsorbent during the adsorption process, 0.25 g/L AS-GO was chosen as the optimal dosage for further research in detail.

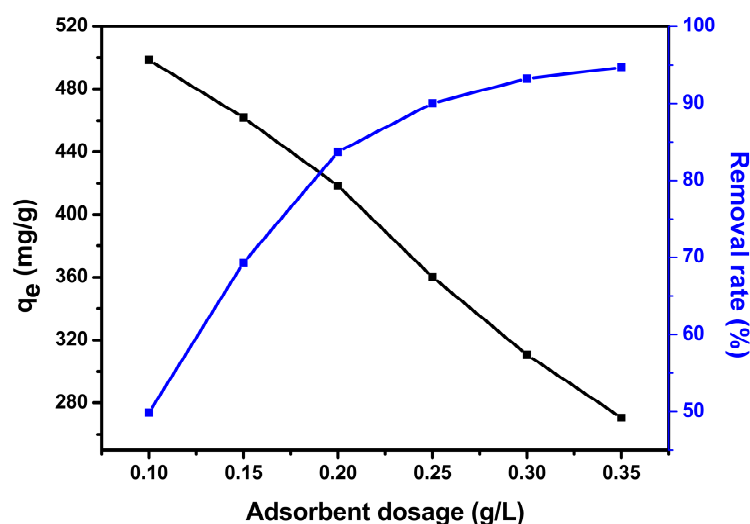


Figure 2. Effect of adsorbent dosage on the removal of OG.

3.1.3. Effect of Chloride Ionic Strength

Chloride ions with high concentrations were often detected in industrial wastewater. It might impact the removal efficiency of AS-GO in practical application. In this study, NaCl was selected as a salt solvent to investigate the effect of chloride ionic strength on the removal of OG (Figure 3). Cl⁻ ionic had an inhibitory effect on the adsorption process. OG removal efficiency decreased obviously from 360.1 to 157.2 mg/g, while Cl⁻ ionic concentration rose from 0 to 100 mmol/L. For one thing, the increasing viscosity and density of solution hindered the adsorption of OG on AS-GO [29]. For another thing, the electrostatic interaction between AS-GO and OG was weakened for the neutralization between the Cl⁻ and the positive adsorption site of AS-GO [30]. The above conclusions indicated that electrostatic interaction was one of the main adsorption mechanisms.

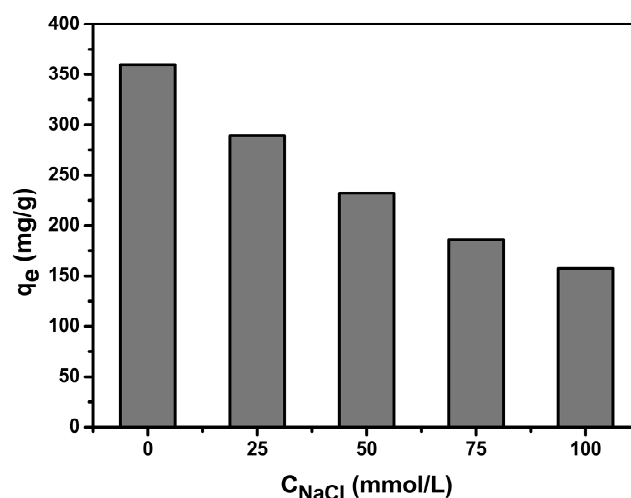


Figure 3. Effect of the ionic strength on the removal of OG.

3.2. Adsorption Isotherm

The adsorption isotherm of OG for AS-GO at 283–313 K was studied. Langmuir and Freundlich adsorption isotherm models were used to explore the adsorption process (Figure 4 and Table 1), respectively. The adsorption capacity was improved with the increment of the initial concentration of OG and came up to equilibrium finally. Meanwhile, high temperature resulted in a high adsorption capacity at the same initial concentration of OG.

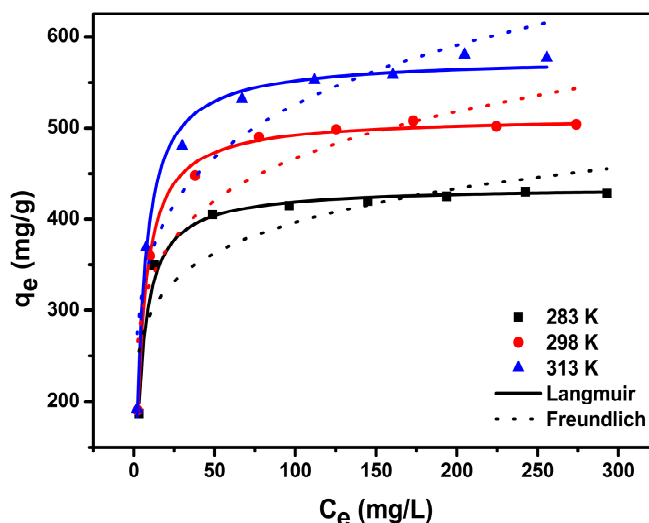


Figure 4. Adsorption isotherms of OG onto AS-GO at various temperatures.

Table 1. Adsorption isotherm parameters for the adsorption of OG onto AS-GO at various temperatures.

Temperature (K)	Langmuir			Freundlich		
	q_{\max} (mg/g)	K_L	R^2	n	K_F	R^2
283	435.8	0.259	0.991	7.81	219.96	0.760
298	512.9	0.240	0.996	6.67	233.59	0.831
313	576.6	0.225	0.991	5.95	242.50	0.875

As can be seen, the Langmuir model was more suitable for the adsorption process than the Freundlich model ($R_L^2 > R_F^2$), indicating that the adsorbed OG was more likely to be dispersed evenly on AS-GO. As indicated by the n values ($0.1 < 1/n < 1$), AS-GO showed a decent adsorption efficiency. Based on the Langmuir model, the maximum adsorption capacities were 435.8, 512.9, and 576.6 mg/g at temperatures of 283, 298 and 313 K, respectively. Table 2 listed the maximal adsorption capacity of OG on various materials in liquid solution in recent years. The q_{\max} of most materials were in the range of 5–400 mg/g, illustrating that AS-GO had potential application prospects for the removal of OG in solution.

Table 2. Comparison of the OG adsorption on various adsorbents.

Adsorbents	pH	q_{\max} (mg/g)	References
graphene–melamine-sponge	-	80.51	[1]
activated carbon	2.0	64.93	[2]
MAMPS	3.0	48.98	[3]
Modified <i>P. coccinea</i>	4.0	57.90	[4]
Fe ₃ O ₄ @catechol/PEI	4.0	192.3	[5]
Fe ₃ O ₄ /MIL-101(Cr)	3.0	200.0	[6]
rGO	2.0	5.98	[7]
Calcined MgAl layered double hydroxides	4.0	665	[8]
magnetic graphene oxide nanocomposite	6.0	20.85	[9]
CLDH	-	378.8	[10]
AS-GO	3.0	576.6	this work

3.3. Adsorption Thermodynamics

For the purpose of further studying the influence of temperature on the adsorption process, experiments were carried out in the temperature range of 283–328 K (in Figure 5), and the thermodynamic parameters including ΔG , ΔH ΔS (in Table 3) were calculated. Negative ΔG at various temperatures facilitated the spontaneous adsorption process. Meanwhile, its absolute values enhanced with the increasing temperature, demonstrating that the increase in temperature motivated the adsorption process. A positive value of ΔS implied that the chaos degree at the solid–liquid interface was increased during the adsorption process. ΔH with a positive value demonstrated that the reaction was endothermic.

Table 3. Thermodynamic parameters for the adsorption of OG onto AS-GO.

Adsorbent	T (K)	ΔG (KJ mol ^{−1})	ΔH (KJ mol ^{−1})	ΔS (J mol ^{−1} K ^{−1})	R^2
AS-GO	283	−7.80	9.79	62.36	0.980
	298	−8.89			
	313	−9.71			
	328	−10.63			

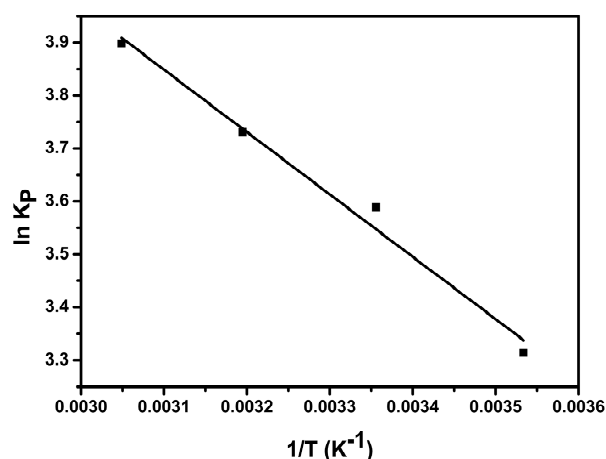


Figure 5. The plot of $\ln K_p$ versus $1/T$ for OG sorption onto AS-GO.

3.4. Adsorption Kinetics

The adsorption kinetics of AS-GO was studied with the initial OG concentration of 50 and 100 mg/L. Figure 6 showed that the adsorption capacity of AS-GO increased over time, ultimately reaching equilibrium within 4 h. When the initial concentration augmented from 50 to 100 mg/L, the adsorption equilibrium time increased from 110 to 280 min.

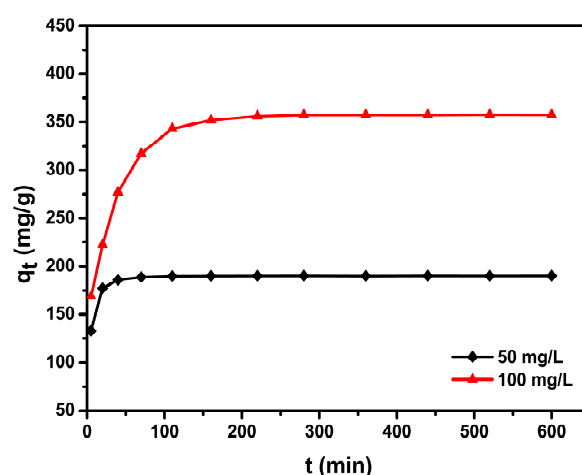


Figure 6. Effect of contact time on the removal of OG at different initial OG concentration.

Two adsorption kinetic models, pseudo-first-order and pseudo-second-order kinetic models, were used to fit the kinetic data to discuss the adsorption mechanisms (Figure 7 and Table 4). The adsorption of OG was discovered to follow the pseudo-second-order kinetic model with great linearity ($R^2 = 0.999$). The low magnification constant of the pseudo-second-order kinetic model explained the rapid adsorption at low initial concentration of OG. Meanwhile, this illustrated that the adsorption rate of OG on AS-GO depended on the chemisorption process.

Table 4. Kinetic parameters for OG adsorption onto AS-GO.

C_0 (mg/L)	$q_{e,exp}$ (mg/g)	Pseudo-First-Order Kinetic Model			Pseudo-Second-Order Kinetic Model		
		k_1	$q_{e,cal}$ (mg/g)	R^2	k_2	$q_{e,cal}$ (mg/g)	R^2
50	190.5	7.97×10^{-3}	4.4	0.568	5.09×10^{-3}	190.8	0.999
100	360.1	7.37×10^{-3}	64.3	0.732	0.33×10^{-3}	364.9	0.999

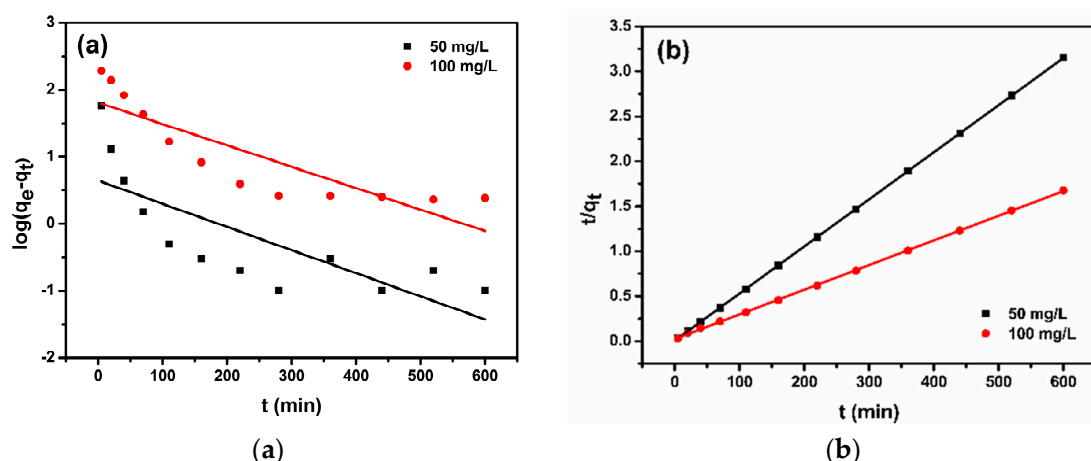


Figure 7. (a) Pseudo–first–order and (b) pseudo–second–order kinetics plots for OG adsorption onto AS-GO.

3.5. Probable Mechanisms

A schematic diagram between AS-GO and OG was visually described in Figure 8. As discussed in the pH effect, electrostatic interaction was one of the adsorption mechanisms. Based on the characterization and experimental data, there were also other mechanisms that affected the adsorption progress.

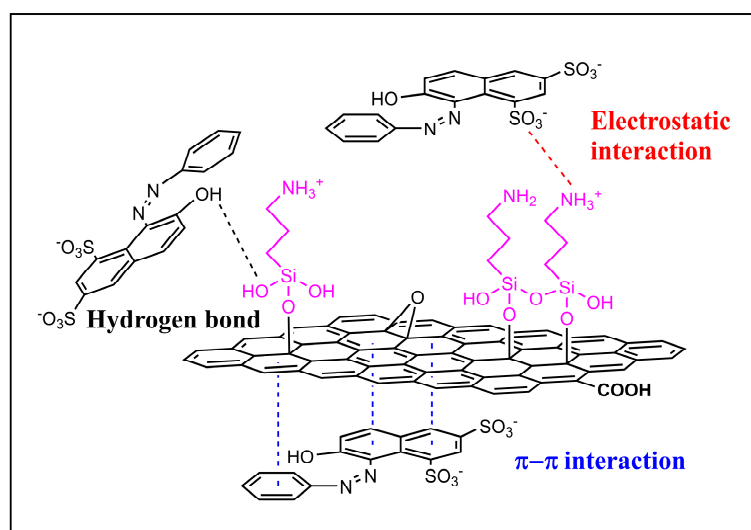


Figure 8. Schematic illustration of adsorption mechanisms by AS-GO.

The FT-IR spectra proved the existence of π - π and hydrogen-bonding interaction (Figure 9). Firstly, the peaks at 1500 and 1221 cm^{-1} were corresponding to the bending vibration of -N=N- and symmetric stretching vibration of -O-S-(O₂), respectively. It indicated that OG was adsorbed onto the surface of AS-GO after the reaction [31,32]. Secondly, the N-H bond characteristic peak (1565 cm^{-1}) shifted to a lower location (1539 cm^{-1}). The peak intensity weakened after reaction, indicating that surface amino of AS-GO participated in the adsorption reaction. Thirdly, the characteristic peaks of O-H and C=C bond at 3431 and 1637 cm^{-1} transferred to 3442 and 1628 cm^{-1} , respectively. π - π interaction might be carried out between the π electron orbit from the C atom of AS-GO and π electrons from the benzene rings of OG. Meanwhile, Si-OH functional groups on the surface of AS-GO might have a hydrogen-bonding interaction with OG [33].

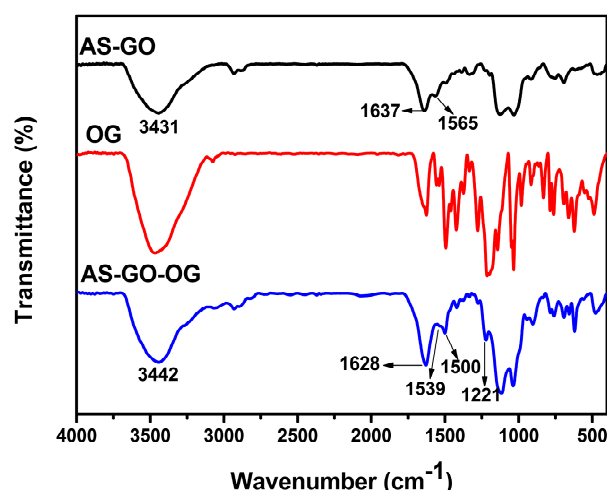


Figure 9. FT-IR spectra of AS-GO, OG and AS-GO-OG.

3.6. Adsorbent Regeneration and Stability

Regeneration and stability of the AS-GO were two key parameters for the evaluation of the adsorption process. Ethanol and deionized water were used as eluents to carry out desorption and re-adsorption experiments. The removal efficiency was kept over 86% after four runs of desorption–adsorption recycling (Figure 10a). Furthermore, there was no significant change in the XRD and FT-IR patterns of AS-GO and AS-GO-OG except for the adsorbed OG spectrum (Figures 8 and 10b). It indicated that the adsorbent had stability. Generally, the AS-GO showed a high potential for the practical application of dye wastewater treatment.

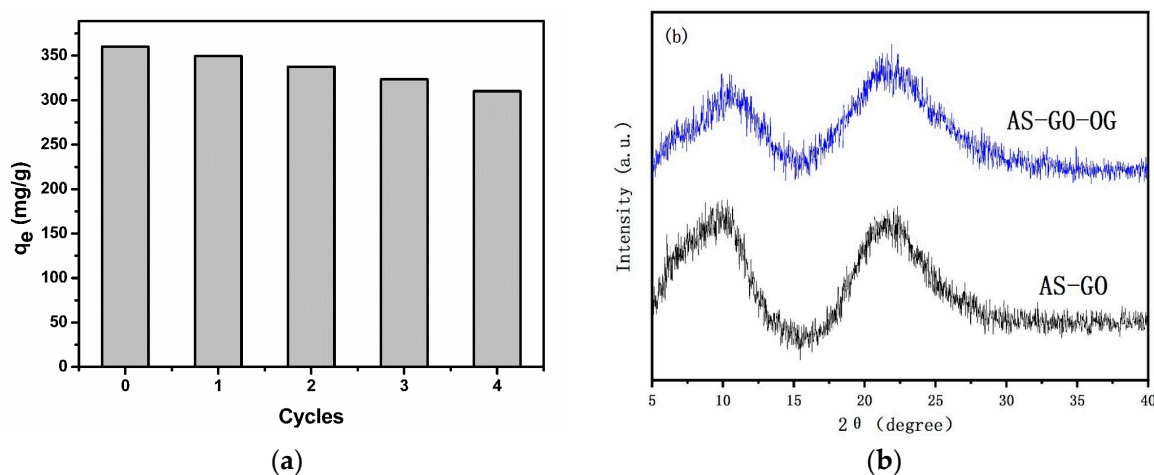


Figure 10. (a) Effect of the cycles on the removal of OG, (b) XRD spectra of AS-GO and AS-GO-OG.

4. Conclusions

In this study, the prepared AS-GO was proved to be a desired sorbent for the treatment of OG effluent in an eco-friendly way. The batch experiments showed that AS-GO had an optimal adsorptive property at the low pH. The high content of chlorine ion inhibited the removal of OG. The Langmuir model represented the isothermal adsorption process better. At 313 K (pH = 3.0), the ceiling amount adsorption capacity was 576.6 mg/g. Adsorption was spontaneous, feasible and endothermic. The pseudo-second-order kinetic model precisely described the OG adsorption kinetic on AS-GO. The adsorption process involved three interactions: Electrostatic interaction, π - π interaction and hydrogen bonding interaction. Consequently, AS-GO was a promising adsorbent, which could be served as a stable and durable adsorbent for the efficient removal of OG from effluents.

Author Contributions: Data curation, W.L. (Wenning Liao) and B.Z.; Funding acquisition, Z.Y.; Investigation, C.H.; Methodology, C.H.; Project administration, Z.Y.; Supervision, Z.Y.; Visualization, W.L. (Wanhui Liu); Writing—original draft, W.L. (Wenning Liao) and X.Z.; Writing—review and editing, Z.Y. All authors have read and agreed to the published version of the manuscript.

Funding: This research was funded by Fundamental Research Funds and National Natural Science Foundation of China (No.51778239) and Open Project of State Key Laboratory of Urban Water Resources and Environment (No. QA201820).

Data Availability Statement: Not applicable.

Acknowledgments: Financial support for this work from Fundamental Research Funds and National Natural Science Foundation of China (No. 51778239) and Open Project of State Key Laboratory of Urban Water Resources and Environment (No. QA201820) was gratefully acknowledged.

Conflicts of Interest: The authors declare no conflict of interest.

References

- Yuksel, A.; Sasaki, M.; Goto, M. Complete degradation of Orange G by electrolysis in sub-critical water. *J. Hazard. Mater.* **2011**, *190*, 1058–1062. [\[CrossRef\]](#) [\[PubMed\]](#)
- Xiao, J.; Lv, W.; Xie, Z.; Tan, Y.; Song, Y.; Zheng, Q. Environmentally friendly reduced graphene oxide as a broad-spectrum adsorbent for anionic and cationic dyes via pi-pi interactions. *J. Mater. Chem. A* **2016**, *4*, 12126–12135. [\[CrossRef\]](#)
- Tekin, D.; Kiziltas, H.; Urgan, H. Kinetic evaluation of ZnO/TiO₂ thin film photocatalyst in photocatalytic degradation of Orange G. *J. Mol. Liq.* **2020**, *306*, 112905. [\[CrossRef\]](#)
- Moghaddas, S.M.T.H.; Elahi, B.; Javanbakht, V. Biosynthesis of pure zinc oxide nanoparticles using Quince seed mucilage for photocatalytic dye degradation. *J. Alloys Compd.* **2020**, *821*, 153519. [\[CrossRef\]](#)
- Liu, M.; Xu, J.; Cheng, B.; Ho, W.; Yu, J. Synthesis and adsorption performance of Mg(OH)(2) hexagonal nanosheet-graphene oxide composites. *Appl. Surf. Sci.* **2015**, *332*, 121–129. [\[CrossRef\]](#)
- Li, W.; Yue, Q.; Gao, B.; Ma, Z.; Li, Y.; Zhao, H. Preparation and utilization of sludge-based activated carbon for the adsorption of dyes from aqueous solutions. *Chem. Eng. J.* **2011**, *171*, 320–327. [\[CrossRef\]](#)
- Abdelkader, N.B.; Bentouami, A.; Derriche, Z.; Bettahar, N.; de Menorval, L.C. Synthesis and characterization of Mg-Fe layer double hydroxides and its application on adsorption of Orange G from aqueous solution. *Chem. Eng. J.* **2011**, *169*, 231–238. [\[CrossRef\]](#)
- Zhu, Z.; Zhang, M.; Liu, F.; Shuang, C.; Zhu, C.; Zhang, Y.; Li, A. Effect of polymeric matrix on the adsorption of reactive dye by anion-exchange resins. *J. Taiwan Inst. Chem. E* **2016**, *62*, 98–103. [\[CrossRef\]](#)
- Wang, Z.; Guo, J.; Ma, J.; Shao, L. Highly regenerable alkali-resistant magnetic nanoparticles inspired by mussels for rapid selective dye removal offer high-efficiency environmental remediation. *J. Mater. Chem. A* **2015**, *3*, 19960–19968. [\[CrossRef\]](#)
- Lawagon, C.P.; Amon, R.E.C. Magnetic rice husk ash ‘cleanser’ as efficient methylene blue adsorbent. *Environ. Eng. Res.* **2020**, *25*, 685–692. [\[CrossRef\]](#)
- Santhosh, C.; Velmurugan, V.; Jacob, G.; Jeong, S.K.; Grace, A.N.; Bhatnagar, A. Role of nanomaterials in water treatment applications: A review. *Chem. Eng. J.* **2016**, *306*, 1116–1137. [\[CrossRef\]](#)
- Banerjee, S.; Dubey, S.; Gautam, R.K.; Chattopadhyaya, M.C.; Sharma, Y.C. Adsorption characteristics of alumina nanoparticles for the removal of hazardous dye, Orange G from aqueous solutions. *Arab. J. Chem.* **2019**, *12*, 5339–5354. [\[CrossRef\]](#)
- Arulkumar, M.; Sathishkumar, P.; Palvannan, T. Optimization of Orange G dye adsorption by activated carbon of Thespesia populnea pods using response surface methodology. *J. Hazard. Mater.* **2011**, *186*, 827–834. [\[CrossRef\]](#) [\[PubMed\]](#)
- Zhang, Z.; Zhang, J.; Liu, J.; Xiong, Z.; Chen, X. Selective and Competitive Adsorption of Azo Dyes on the Metal-Organic Framework ZIF-67. *Water Air Soil Pollut.* **2016**, *227*, 471. [\[CrossRef\]](#)
- Hu, H.; Wageh, S.; Al-Ghamdi, A.A.; Yang, S.; Tian, Z.; Cheng, B.; Ho, W. NiFe-LDH nanosheet/carbon fiber nanocomposite with enhanced anionic dye adsorption performance. *Appl. Surf. Sci.* **2020**, *511*, 145570. [\[CrossRef\]](#)
- Xu, M.; Jiang, H.; Xie, Z.; Li, Z.; Xu, D.; He, F. Highly efficient selective adsorption of anionic dyes by modified beta-cyclodextrin polymers. *J. Taiwan Inst. Chem. E* **2020**, *108*, 114–128. [\[CrossRef\]](#)
- He, J.; Ni, F.; Cui, A.; Chen, X.; Deng, S.; Shen, F.; Huang, C.; Yang, G.; Song, C.; Zhang, J.; et al. New insight into adsorption and co-adsorption of arsenic and tetracycline using a Y-immobilized graphene oxide-alginate hydrogel: Adsorption behaviours and mechanisms. *Sci. Total Environ.* **2020**, *701*, 134363. [\[CrossRef\]](#)
- Bao, S.; Yang, W.; Wang, Y.; Yu, Y.; Sun, Y. One-pot synthesis of magnetic graphene oxide composites as an efficient and recoverable adsorbent for Cd(II) and Pb(II) removal from aqueous solution. *J. Hazard. Mater.* **2020**, *381*, 120914. [\[CrossRef\]](#)
- Yin, W.; Zhan, X.; Fang, P.; Xia, M.; Yu, J.; Chi, R. A Facile One-Pot Strategy to Functionalize Graphene Oxide with Poly(amino-phosphonic Acid) Derived from Wasted Acrylic Fibers for Effective Gd(III) Capture. *ACS Sustain. Chem. Eng.* **2019**, *7*, 19857–19869. [\[CrossRef\]](#)
- Madadrang, C.J.; Kim, H.Y.; Gao, G.; Wang, N.; Zhu, J.; Feng, H.; Gorrning, M.; Kasner, M.L.; Hou, S. Adsorption Behavior of EDTA-Graphene Oxide for Pb (II) Removal. *ACS Appl. Mater. Interfaces* **2012**, *4*, 1186–1193. [\[CrossRef\]](#)

21. Wang, Z.; Gao, M.; Li, X.; Ning, J.; Zhou, Z.; Li, G. Efficient adsorption of methylene blue from aqueous solution by graphene oxide modified persimmon tannins. *Mater. Sci. Eng. C. Mater. Biol. Appl.* **2020**, *108*, 110196. [[CrossRef](#)]
22. Xue, A.; Zhou, S.; Zhao, Y.; Lu, X.; Han, P. Effective NH₂-grafting on attapulgite surfaces for adsorption of reactive dyes. *J. Hazard. Mater.* **2011**, *194*, 7–14. [[CrossRef](#)]
23. Lima, V.V.C.; Nora, F.B.D.; Peres, E.C.; Reis, G.S.; Lima, E.C.; Oliveira, M.L.S.; Dotto, G.L. Synthesis and characterization of biopolymers functionalized with APTES (3-aminopropyltriethoxysilane) for the adsorption of sunset yellow dye. *J. Environ. Chem. Eng.* **2019**, *7*. [[CrossRef](#)]
24. Cote, L.J.; Kim, F.; Huang, J. Langmuir-Blodgett Assembly of Graphite Oxide Single Layers. *J. Am. Chem. Soc.* **2009**, *131*, 1043–1049. [[CrossRef](#)] [[PubMed](#)]
25. He, C.; Yang, Z.; Ding, J.; Chen, Y.; Tong, X.; Li, Y. Effective removal of Cr(VI) from aqueous solution by 3-aminopropyltriethoxysilane-functionalized graphene oxide. *Colloid Surf. A* **2017**, *520*, 448–458. [[CrossRef](#)]
26. Li, T.; Yang, Z.; Zhang, X.; Zhu, N.; Niu, X. Perchlorate removal from aqueous solution with a novel cationic metal–organic frameworks based on amino sulfonic acid ligand linking with Cu-4,4'-bipyridyl chains. *Chem. Eng. J.* **2015**, *281*, 1008–1016. [[CrossRef](#)]
27. Atia, A.A.; Donia, A.M.; Al-Amrani, W.A. Adsorption/desorption behavior of acid orange 10 on magnetic silica modified with amine groups. *Chem. Eng. J.* **2009**, *150*, 55–62. [[CrossRef](#)]
28. Zhou, Q.; Chen, F.; Wu, W.; Bu, R.; Li, W.; Yang, F. Reactive orange 5 removal from aqueous solution using hydroxyl ammonium ionic liquids/layered double hydroxides intercalation composites. *Chem. Eng. J.* **2016**, *285*, 198–206. [[CrossRef](#)]
29. Yang, S.; Hu, J.; Chen, C.; Shao, D.; Wang, X. Mutual Effects of Pb(II) and Humic Acid Adsorption on Multiwalled Carbon Nanotubes/Polyacrylamide Composites from Aqueous Solutions. *Environ. Sci. Technol.* **2011**, *45*, 3621–3627. [[CrossRef](#)] [[PubMed](#)]
30. Vilar, V.; Botelho, C.; Boaventura, R. Influence of pH, ionic strength and temperature on lead biosorption by Gelidium and agar extraction algal waste. *Process. Biochem.* **2005**, *40*, 3267–3275. [[CrossRef](#)]
31. Gao, J.; Zhang, L.; Liu, X.; Zhang, W. Hierarchically structured, well-dispersed Ti⁴⁺ cross-linked chitosan as an efficient and recyclable sponge-like adsorbent for anionic azo-dye removal. *RSC Adv.* **2016**, *6*, 106260–106267. [[CrossRef](#)]
32. Zhang, L.; Cheng, Z.; Guo, X.; Jiang, X.; Liu, R. Process optimization, kinetics and equilibrium of orange G and acid orange 7 adsorptions onto chitosan/surfactant. *J. Mol. Liq.* **2014**, *197*, 353–367. [[CrossRef](#)]
33. Wu, Z.; Zhong, H.; Yuan, X.; Wang, H.; Wang, L.; Chen, X.; Zeng, G.; Wu, Y. Adsorptive removal of methylene blue by rhamnolipid-functionalized graphene oxide from wastewater. *Water Res.* **2014**, *67*, 330–344. [[CrossRef](#)] [[PubMed](#)]